The Plant Cell, Vol. 29: 589–599, March 2017, www.plantcell.org

IDN2 Interacts with RPA and Facilitates DNA Double-Strand Break Repair by Homologous Recombination in Arabidopsis

Mingming Liu,[a,b] Zhaoqing Ba,[c] Pedro Costa-Nunes,[d,1] Wei Wei,[c] Lanxia Li,[c] Fansi Kong,[e] Yan Li,[c] Jijie Chai,[c,f] Olga Pontes,[d] and Yijun Qi[c,f,2]

[a] Peking University-Tsinghua University-National Institute of Biological Sciences Joint Graduate Program, School of Life Sciences, Peking University, Beijing 100871, China
[b] National Institute of Biological Sciences, Beijing 102206, China
[c] Center for Plant Biology, School of Life Sciences, Tsinghua University, Beijing 100084, China
[d] Shanghai Center for Plant Stress Biology, Shanghai Institute for Biological Sciences, Chinese Academy of Sciences, Shanghai 200032, China
[e] Bionova (Beijing) Biotech Co., Beijing 102206, China
[f] Tsinghua-Peking Center for Life Sciences, Beijing 100084, China

ORCID IDs: 0000-0002-9348-8994 (M.L.); 0000-0002-2033-6519 (P.C.-N.); 0000-0002-7100-1700 (Y.Q.)

Repair of DNA double-strand breaks (DSBs) is critical for the maintenance of genome integrity. We previously showed that DSB-induced small RNAs (diRNAs) facilitate homologous recombination-mediated DSB repair in *Arabidopsis thaliana*. Here, we show that INVOLVED IN DE NOVO2 (IDN2), a double-stranded RNA binding protein involved in small RNA-directed DNA methylation, is required for DSB repair in Arabidopsis. We find that IDN2 interacts with the heterotrimeric replication protein A (RPA) complex. Depletion of IDN2 or the diRNA binding ARGONAUTE2 leads to increased accumulation of RPA at DSB sites and mislocalization of the recombination factor RAD51. These findings support a model in which IDN2 interacts with RPA and facilitates the release of RPA from single-stranded DNA tails and subsequent recruitment of RAD51 at DSB sites to promote DSB repair.

INTRODUCTION

DNA double-strand breaks (DSBs) are serious genetic lesions generated by ionizing radiation (IR) and various endogenous or exogenous insults, which can lead to genome instability and even cell death if unrepaired or repaired incorrectly. Cells have evolved two major pathways to repair DSBs: the nonhomologous end joining and homologous recombination (HR) pathways (Puchta, 2005; San Filippo et al., 2008; Ciccia and Elledge, 2010; Lieber, 2010; Moynahan and Jasin, 2010). Nonhomologous end joining is an error-prone process that mediates the direct ligation of the two DSB ends, potentially introducing short deletions or insertions (Lieber, 2010). HR ensures error-free repair but requires homologous chromosome or sister chromatids as a template (San Filippo et al., 2008; Moynahan and Jasin, 2010).

HR initiates with 5′ to 3′ end resection of DSB ends by the MRE11-RAD50-NBS1 complex (van den Bosch et al., 2003), CtBP-interacting protein (Sartori et al., 2007), and EXONUCLEASE1 (Mimitou and Symington, 2008) to produce single-stranded DNA (ssDNA) tails. ssDNA tails are bound by the heterotrimeric protein complex RPA, which consists of three subunits: RPA1, RPA2, and RPA3 (San Filippo et al., 2008; Krejci et al., 2012; Chen and Wold, 2014). RPAs are then replaced by the recombinase RAD51 to assemble nucleoprotein filaments facilitating homology search, strand invasion, and subsequent HR events (San Filippo et al., 2008; Krejci et al., 2012).

Small RNAs, which are processed by DICER or DICER-LIKE (DCL) proteins from double-stranded RNAs (dsRNAs) and are associated with ARGONAUTE (AGO) family proteins, play important regulatory roles in diverse biological processes (Fang and Qi, 2016). We and others have previously reported that DSBs can trigger the production of a class of small RNAs derived from the sequences around the DSB sites in *Arabidopsis thaliana* (Wei et al., 2012) and mammals (Francia et al., 2012; Wei et al., 2012). These DSB-induced small RNAs (diRNAs) associate with AGO proteins and promote HR repair (Wei et al., 2012; Gao et al., 2014).

In Arabidopsis, the generation of diRNAs requires plant-specific RNA polymerase IV (Pol IV), RNA-dependent RNA polymerase proteins, and DCL proteins (Wei et al., 2012). This is analogous to how 24-nucleotide heterochromatic small interfering RNAs (hc-siRNAs) are produced in the RNA-directed DNA methylation (RdDM) pathway (Law and Jacobsen, 2010; Zhang and Zhu, 2011; Matzke and Mosher, 2014; Wendte and Pikaard, 2017). Although diRNAs associate with AGO2 and do not use the RdDM pathway, in which hc-siRNAs associate with AGO4 (Zilberman et al., 2003; Qi et al., 2006) to facilitate DSB repair, other components involved in the RdDM pathway, e.g., Pol V, play a role in DSB repair (Wei et al., 2012). These findings suggest that the RdDM pathway shares components with diRNA-mediated DSB repair. A recent study has also provided a link between the nucleotide excision repair machinery and the RdDM pathway (Schalk et al., 2016). DNA DAMAGE BINDING2, a protein that is involved in nucleotide excision repair, influences de novo DNA methylation through interacting with AGO4 and controlling the local abundance of hc-siRNAs (Schalk et al., 2016).

[1] Current address: Donald Danforth Plant Science Center, St. Louis, MO 63132.
[2] Address correspondence to qiyijun@tsinghua.edu.cn.
The author responsible for distribution of materials integral to the findings presented in this article in accordance with the policy described in the Instructions for Authors (www.plantcell.org) is: Yijun Qi (qiyijun@tsinghua.edu.cn).
www.plantcell.org/cgi/doi/10.1105/tpc.16.00769

It has been shown that INVOLVED IN DE NOVO2 (IDN2), a dsRNA binding protein (Ausin et al., 2009; Zheng et al., 2010; Schalk et al., 2016), forms a complex with IDN2 paralog 1 (IDP1) and IDP2 that functions at the effector stage of RdDM (Ausin et al., 2012; Xie et al., 2012; Zhang et al., 2012). In this study, we found that IDN2 was involved in HR repair and that its dsRNA binding activity was required for its function in HR repair. IDN2 interacted with RPA, and depletion of IDN2 or AGO2 resulted in overaccumulation of RPA at DSB sites and mislocalization of RAD51. Our findings suggest that IDN2 is recruited to DSB sites, likely by AGO2/diRNA complexes, and facilitates the dissociation of RPA from ssDNA tails via protein-protein interaction, thereby promoting the loading of RAD51 onto DSBs

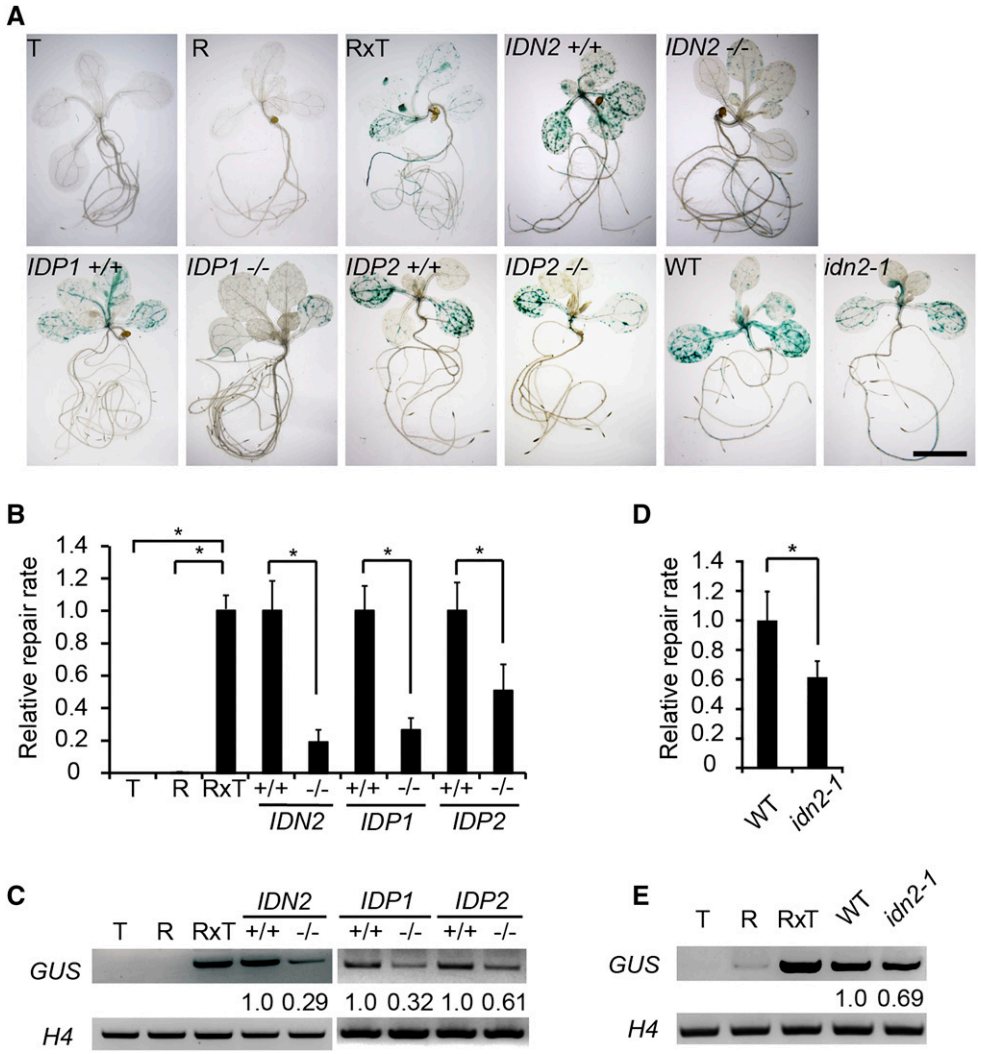

Figure 1. The IDN2 Complex Is Required for DSB Repair.

(A) Representative GUS staining images illustrating DSB repair rates. Photographs show GUS staining in the T, R, and RxT lines and in the RxT lines either in the *idn2-3*, *idp1-1*, *idp2-1*, or *idn2-1* mutant (−/−) backgrounds or in their corresponding wild-type (+/+) backgrounds. The intensity of GUS staining in the plants represents the rate of DSB repair. Bar = 5 mm

(B) The relative DSB repair rates in the indicated plants as determined by GUS staining. At least 30 plants in each genetic background from three independent experiments were stained and blue sectors were counted. The repair efficiency in the corresponding wild type (+/+) was arbitrarily set to 1.0. The repair rates in the indicated mutants (−/−) are presented relative to those of the corresponding wild type. Error bars indicate SE, and the asterisks indicate significant differences between two groups (*t* test, $P < 0.001$).

(C) Detection of repaired DNA in the indicated plants by PCR. Genomic DNA was digested with I-*SceI* and used for PCR detection of the repaired *GUS* fragment. Histone *H4* was also amplified as a control. The intensities of *GUS* PCR bands were quantified and abundances relative to the wild type (set at 1.0) are shown below the gel lanes.

(D) DSB repair rates determined by GUS staining as described in **(B).**

(E) DSB repair rates determined by PCR in the indicated plants as described in **(C)**.

RESULTS

IDN2 and Its Two Paralogs Are Involved in DSB Repair

Our previous study suggested that diRNA-mediated HR repair shares protein components with the RdDM pathway (Wei et al., 2012). We thus explored the role of IDN2 and its two paralogs IDP1 and IDP2, which act downstream of RdDM in HR repair. We examined the HR repair rate using a well-established DGU.US system in *idn2-3*, *idp1-1*, and *idp2-1* mutant backgrounds. This system uses the DGU.US reporter (R) line, which contains a unique I-*Sce*I recognition site within the direct repeats in conjunction with the DSB-triggering (T) line that expresses the endonuclease I-*Sce*I. In the crossed (R×T) line, DSBs are generated at the I-*Sce*I site, and the repair of DSBs results in restored expression of GUS and color production in histochemical assays (Orel et al., 2003;

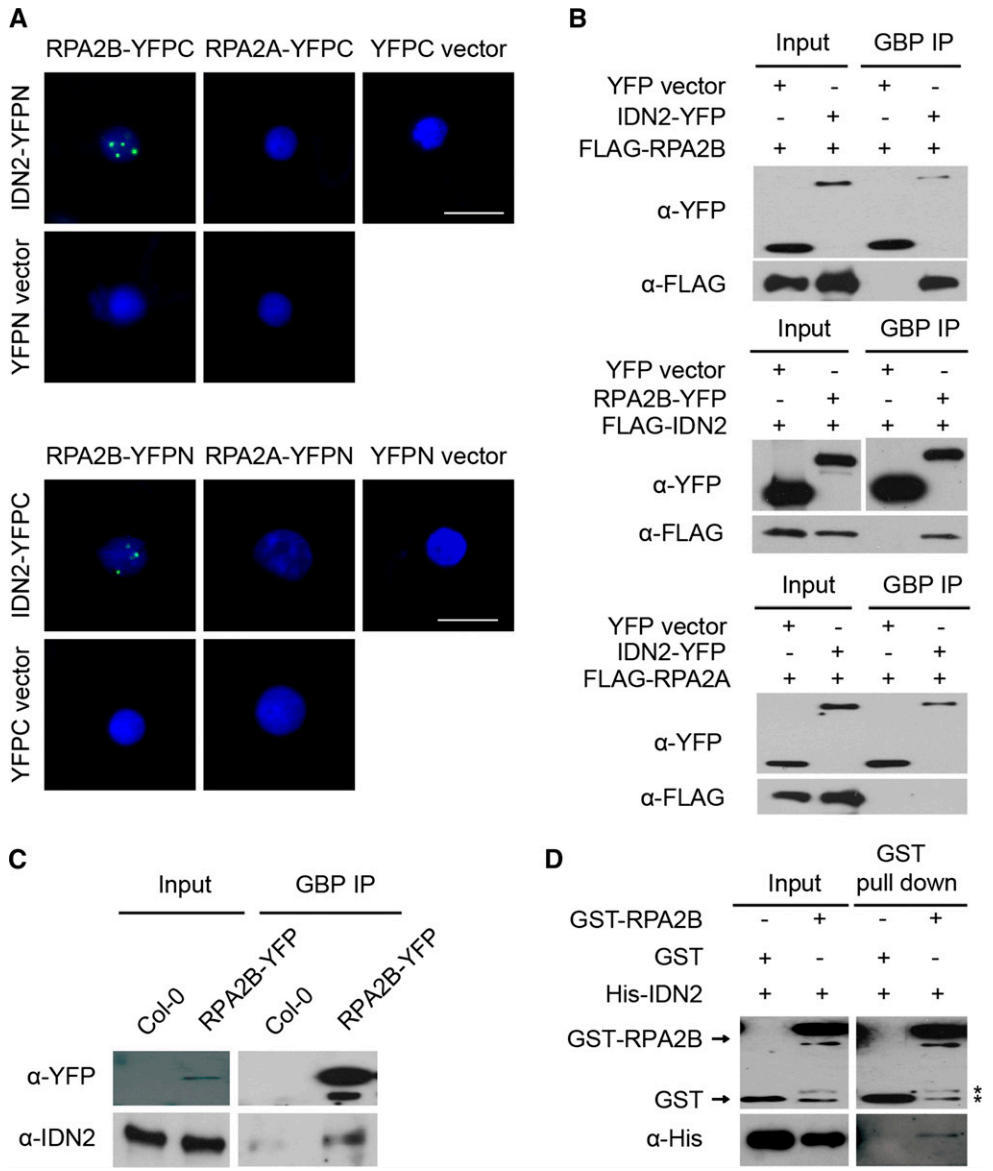

Figure 2. IDN2 Interacts with RPA2B.

(A) Detection of the interactions between IDN2 and RPA2B by BiFC. *N. benthamiana* leaves were infiltrated with agrobacteria transformed with indicated constructs and examined by fluorescence microscopy. RPA2B but not RPA2A interacted with IDN2 and formed foci in the nuclei. Bar = 20 μm.
(B) Detection of the interaction between IDN2 and RPA2B in Arabidopsis protoplasts. Protoplasts transiently expressing the tagged proteins listed above the panels were analyzed by coimmunoprecipitation using GFP binding protein (GBP)-conjugated beads and the antibodies noted to the left.
(C) Detection of the interaction between IDN2 and RPA2B in transgenic plants. IDN2 was detected in RPA2B-YFP immunoprecipitates that were prepared from a transgenic line expressing RPA2B-YFP under its native promoter using a homemade IDN2 antibody.
(D) Detection of the direct interaction between IDN2 and RPA2B using a GST pull-down assay. Asterisks indicate nonspecific bands.

Mannuss et al., 2010). *IDN2* mutation caused a significant reduction in HR repair efficiency, as measured either by GUS staining or by PCR detection of the repaired *GUS* gene (Supplemental Figures 1 to 2; Figures 1A to 1C). *IDP1* and *IDP2* mutations also led to reduction of DSB repair rate, albeit to a lesser extent (Supplemental Figures 3 and 4; Figures 1A to 1C). Our results suggest that IDN2, IDP1, and IDP2 are all involved in DSB repair. This is not surprising as IDN2, IDP1, and IDP2 form a functional complex (Ausin et al., 2012; Xie et al., 2012; Zhang et al., 2012).

IDN2 binds dsRNA in vitro (Ausin et al., 2009; Zhang et al., 2012) and associates with Pol V-dependent scaffold transcripts in vivo (Zhu et al., 2013; Bohmdorfer et al., 2014). To determine whether RNA binding is critical for the role of IDN2 in HR repair, we

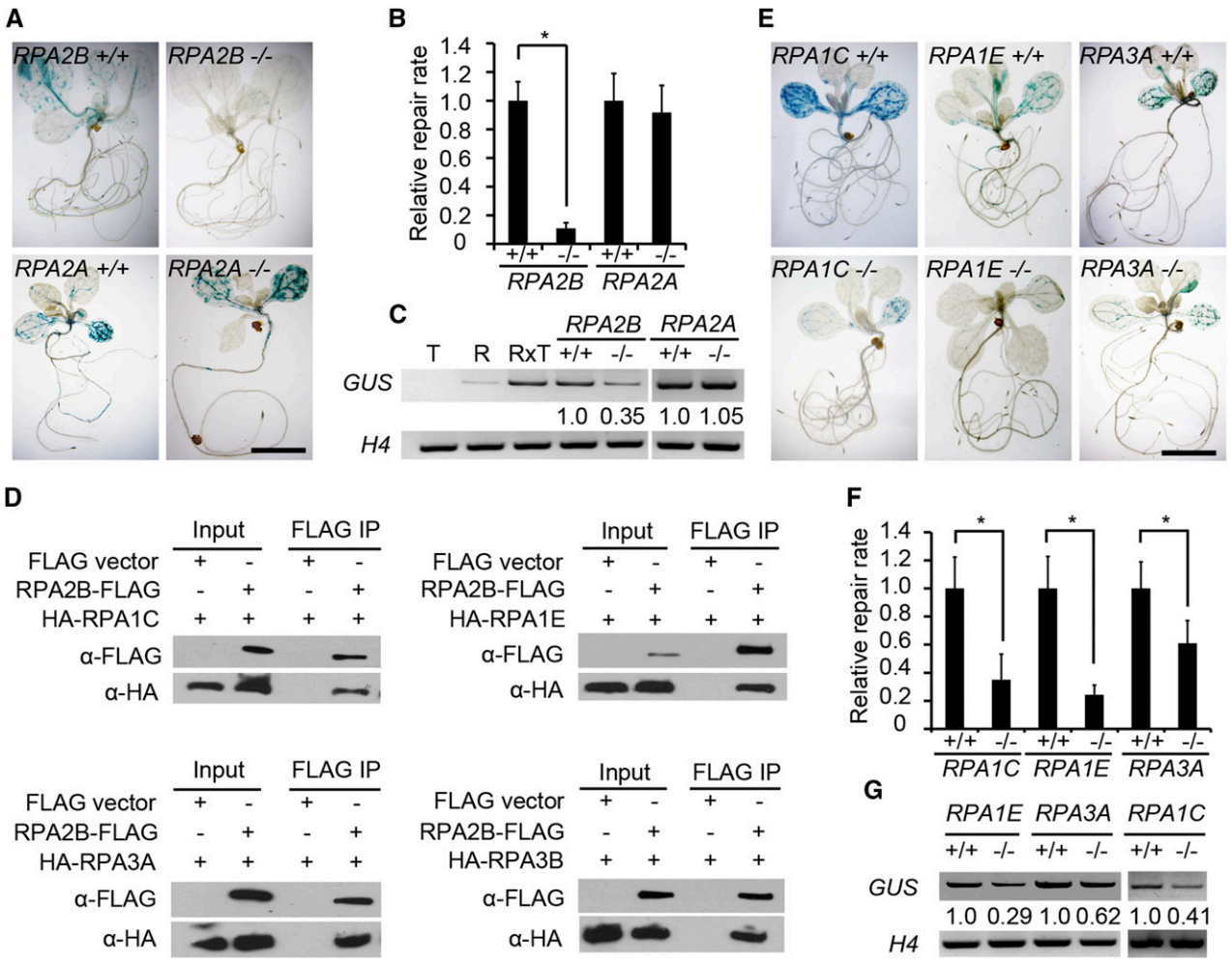

Figure 3. Identification of the RPA Complex Required for DSB Repair.

(A) Representative GUS staining images illustrating DSB repair rates. Photographs show GUS staining in the *rpa2b-1* or *rpa2a-1* mutant (−/−) background and in their corresponding wild-type (+/+) backgrounds. Bar = 5 mm.

(B) The relative DSB repair rates in the indicated plants as determined by GUS staining. At least 30 plants in each genetic background from three independent experiments were stained and blue sectors were counted. Error bars indicate SE, and the asterisk shows a significant difference between two groups (*t* test, $P < 0.001$).

(C) Detection of repaired DNA by PCR. Genomic DNA was digested with I-*SceI* and used for PCR detection of the repaired *GUS* fragment. Histone *H4* was also amplified as a control. The intensities of *GUS* PCR bands were quantified and abundances relative to wild type (set at 1.0) are shown below the gel lanes

(D) Detection of interactions between RPA2B and RPA1C, RPA1E, RPA3A, or RPA3B in Arabidopsis protoplasts. Protoplasts transiently expressing the tagged proteins listed above the panels were analyzed by coimmunoprecipitation using anti-FLAG M2 magnetic beads and the antibodies noted to the left.

(E) Representative GUS staining images illustrating DSB repair rates. Photographs show GUS staining in the *rpa1c-1*, *rpa1e-1*, or *rpa3a-1* mutant (−/−) background and in their corresponding wild-type (+/+) backgrounds. Bar = 5 mm.

(F) The relative DSB repair rates in the indicated plants as determined by GUS staining. At least 30 plants in each genetic background from three independent experiments were stained and blue sectors were counted. Error bars indicate SE, and asterisks indicate significant differences between two groups (*t* test, $P < 0.001$).

(G) Detection of repaired DNA in the indicated plants by PCR as described in **(C)**.

determined the rate of DSB repair in the *idn2-1* mutant, which carries a point mutation followed by a 24-bp deletion in its XS domain (Fukunaga and Doudna, 2009), which binds dsRNA. This leads to the expression of a mutant form of IDN2 that is defective in RNA binding ability (Ausin et al., 2009; Zhu et al., 2013). The HR repair rate was reduced by 30 to 40% in the *idn2-1* mutant plants relative to wild-type plants (Supplemental Figure 5; Figures 1A, 1D, and 1E), suggesting that RNA binding activity of IDN2 may partially contribute to its role in DSB repair. It is noteworthy that the *idn2-1* mutation also leads to decreased accumulation of IDN2 (Zhu et al., 2013). Thus, we cannot rule out the possibility that the reduced HR repair rate in *idn2-1* could be also partially attributed to the decreased level of IDN2.

IDN2 Is Not Required for diRNA Production

Our previous study showed the DSB repair efficiency is highly compromised in mutants defective in diRNA accumulation (Wei et al., 2012). To test whether reduced DSB repair rate in the *idn2* mutants was due to decreased production of diRNAs, we performed RNA gel blot analyses but found that the *idn2-3* mutant accumulated much more diRNAs than did wild-type plants and that the *idn2-1* mutant had a lesser increase in diRNA accumulation (Supplemental Figures 6A to 6C). Thus, it is unlikely that the reduced HR repair rate in *idn2* can be attributed to impaired diRNA production. The increased amount of diRNAs in the *idn2-3* mutant is similar to that caused by *Pol V* mutation (Wei et al., 2012). It is possible that mutation of the RdDM components alleviates silencing of the transgenic locus, thereby providing more substrates for diRNA production.

IDN2 Interacts with RPA2B

To further dissect how IDN2 facilitates DSB repair, we performed bimolecular fluorescence complementation (BiFC) assays in tobacco (*Nicotiana benthamiana*) leaves to identify protein-protein interactions between IDN2 and key proteins involved in major steps of HR. These proteins included MRE11, RAD50, RPA, and RAD51. To analyze protein interactions in an unbiased manner, we included all of RPA subunits in our BiFC assays. Our results showed that IDN2 did not interact with MRE11 and RAD51 (Supplemental Figure 7). To our surprise, IDN2 interacted with RPA2B (Figure 2A). Interactions between IDN2 and other RPA subunits, e.g., RPA2A, were not observed, suggesting a specific association between IDN2 and RPA2B (Figure 2A; Supplemental Figure 7). To confirm these observations, we performed reciprocal coimmunoprecipitation experiments using Arabidopsis protoplasts transiently expressing tagged IDN2 and RPA subunits. We

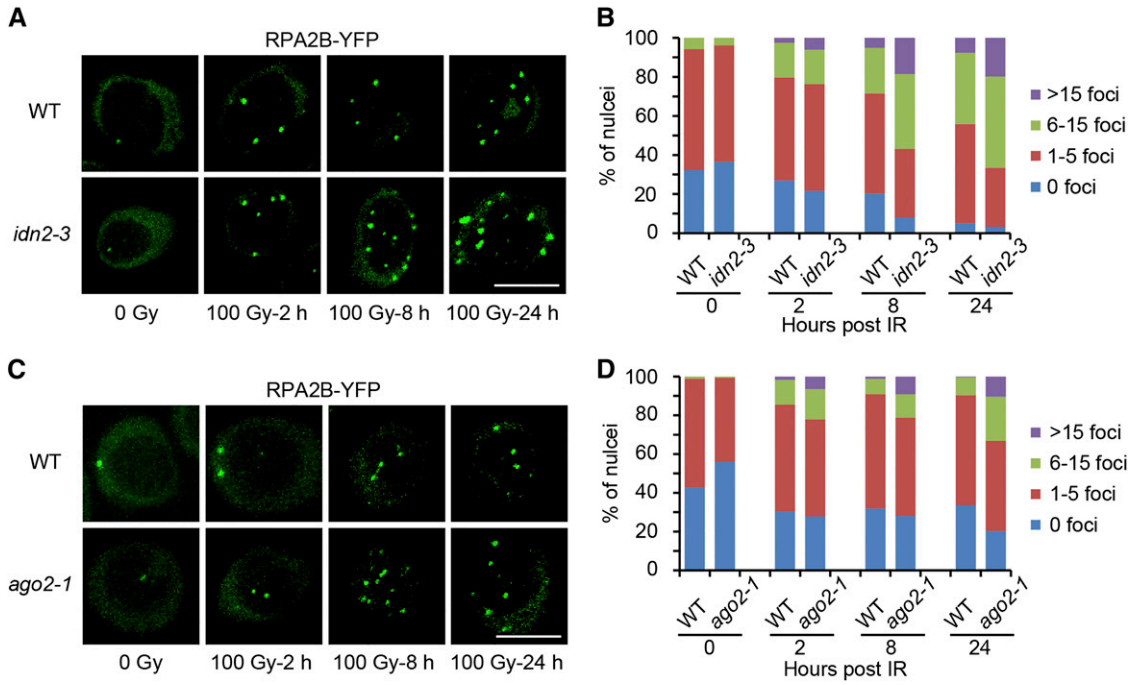

Figure 4. IDN2 and AGO2 Dysfunction Causes Overaccumulation of RPA2B Foci.

(A) Representative images showing RPA2B-YFP foci in live root tip cells in wild-type and *idn2-3* plants. Images were taken from the root tips of 5-d-old seedlings at the indicated time points post γ-irradiation (100 Gy) by a confocal microscope. Bar = 10 μm.

(B) Graphic representation of the number of RPA2B-GFP foci detected in the indicated plants in **(A)**. The numbers of foci in at least 400 nuclei from eight root tips were counted for each sample and used to generate the diagram.

(C) Representative images showing RPA2B-YFP foci in live root tip cells in wild-type and *ago2-1* plants. Images were taken as described in **(A)**. Bar = 10 μm.

(D) Graphic representation of the number of RPA2B-GFP foci detected in the indicated plants in **(C)**. The numbers of foci in at least 400 nuclei from eight root tips were counted for each sample and used to generate the diagram.

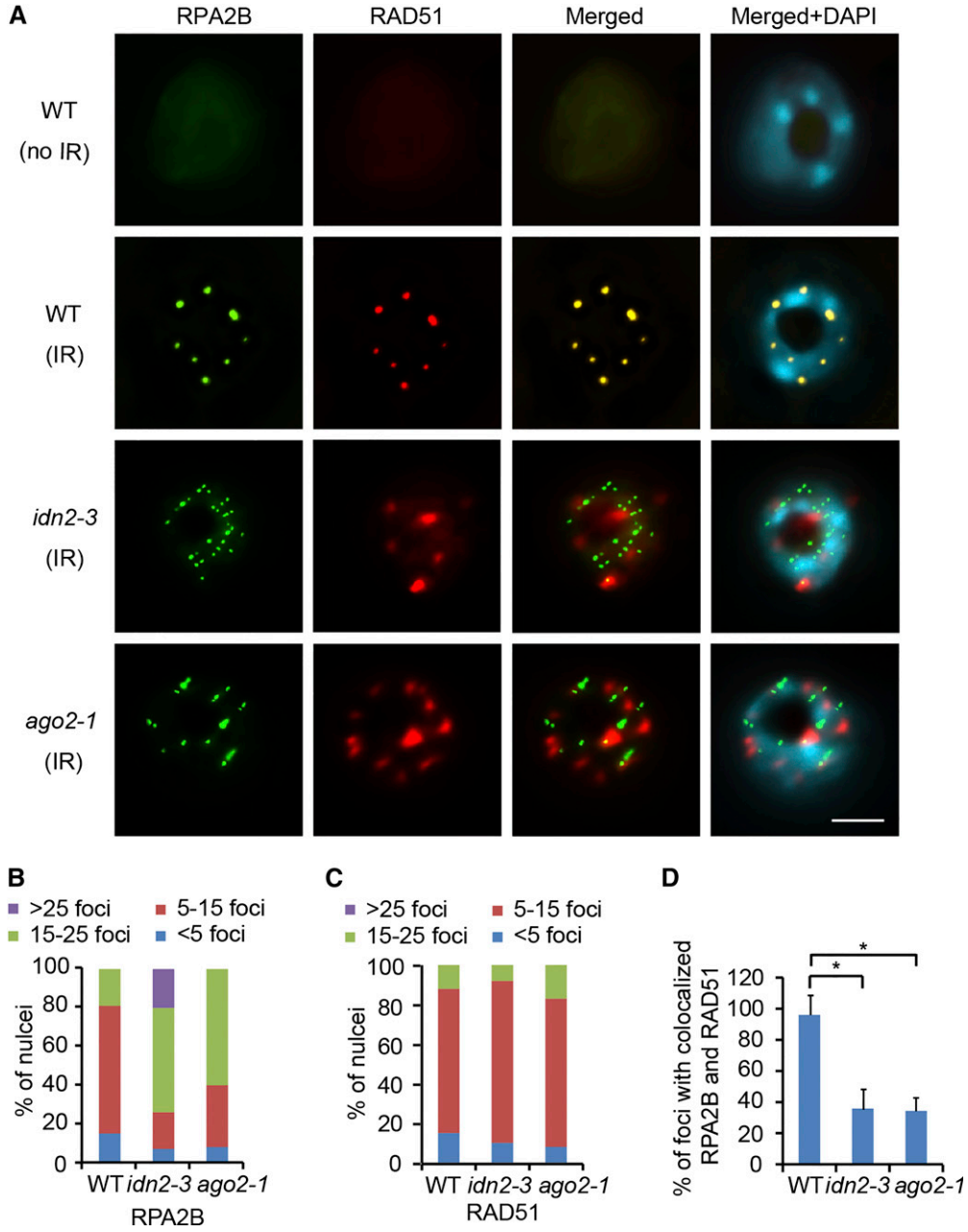

Figure 5. Depletion of IDN2 or AGO2 Causes Mislocalization of RAD51.

(A) Detection of RPA2B-YFP and RAD51 foci formed in the nuclei of leaf cells. Representative images using unirradiated (no IR) or irradiated (IR) wild-type, *idn2-3*, and *ago2-1* mutant plants expressing RPA2B-YFP are shown. DNA is stained with DAPI (blue). Merged images overlay RPA2B (green) and RAD51 (red). Bar = 5 μm.
(B) Graphic representation of the number of RPA2B-YFP foci detected in the indicated plants. The numbers of foci in at least 60 nuclei from two independent experiments were counted for each sample and used to generate the diagram.
(C) Graphic representation of the number of RAD51 foci detected in the indicated plants. The numbers of foci in at least 60 nuclei from two independent experiments were counted for each sample and used to generate the diagram.
(D) The percentage of colocalized RPA2B-YFP and RAD51 foci in the indicated plants. Error bars indicate SE, and the asterisks indicate significant differences between two groups (*t* test, $P < 0.001$). The numbers of foci in at least 60 nuclei from two independent experiments were counted for each sample to generate the diagram.

found that FLAG-RPA2B but not FLAG-RPA2A was coimmunoprecipitated with IDN2-YFP and that FLAG-IDN2 was coimmunoprecipitated with RPA2B-YFP (Figure 2B). Moreover, we did the coimmunoprecipitation experiment using the transgenic RPA2B-YFP plants and found that endogenous IDN2 was coimmunoprecipitated with RPA2B-YFP (Figure 2C). To further examine whether the interaction between IDN2 and RPA2B is direct, we performed a GST pull-down assay and found that

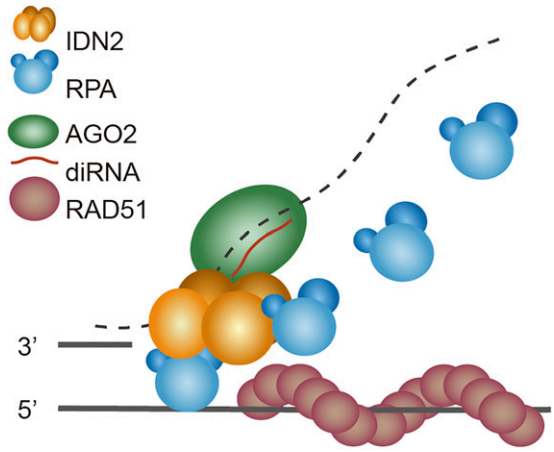

Figure 6. A Model for the Role of IDN2 in diRNA-Mediated HR Repair in Arabidopsis.

In this model, AGO2/diRNA complexes are recruited to DSBs through base pairing with nascent transcripts, which provides dsRNA structures for IDN2 binding. IDN2 complexes interact with RPA complexes and facilitate their dissociation from DSB ends, thereby promoting the formation of RAD51 filaments to mediate HR repair.

His-tagged IDN2 specifically bound GST-RPA2B (Figure 2D). Taken together, our data indicate that IDN2 and RPA2B directly interact.

The RPA Complex Is Required for DSB Repair

The RPA complex is formed by RPA1, RPA2, and RPA3 subunits. It binds ssDNA tails generated from DSBs and is essential for DSB repair (San Filippo et al., 2008; Krejci et al., 2012; Chen and Wold, 2014). The Arabidopsis genome encodes five RPA1 homologs (A–E), two RPA2 homologs (A and B), and two RPA3 homologs (A and B) (Aklilu et al., 2014) (Supplemental Figure 8 and Supplemental File 1). Among them, RPA1A, RPA1C, and RPA1E have been shown to be induced by IR (Culligan et al., 2006). In an attempt to verify role of RPA subunits in HR repair, we first examined the HR repair rate in wild-type, *rpa2a-1*, and *rpa2b-1* mutant backgrounds. *RPA2B* mutation led to diminished DSB repair (Figures 3A to 3C), suggesting that RPA2B is an essential subunit of the RPA complex for DSB repair. By contrast, *RPA2A* mutation had no effect on DSB repair rate (Figures 3A to 3C). Different homologs of RPA subunits may form distinct RPA complexes with different functions (Eschbach and Kobbe, 2014). To find out the partners of RPA2B in DSB repair, we again performed BiFC and found that RPA2B formed a complex with either RPA1C or RPA1E and either RPA3A or RPA3B (Supplemental Figure 9). Notably, the interactions were verified via coimmunoprecipitation assay in Arabidopsis protoplasts transiently expressing tagged proteins (Figure 3D). Consistent with the protein interaction results, HR repair rates also declined in the *rpa1c-1*, *rpa1e-1*, and *rpa3a-1* mutants (Figures 3E to 3G), suggesting that the RPA complex is important for HR repair. We expect that the *rpa3b* mutant would also display defects in DSB repair, but, due to lack of *rpa3b* mutant, we were unable to determine this.

Depletion of IDN2 or AGO2 Leads to Overaccumulation of RPA2B Foci

IDN2 appears to serve as an adapter between scaffold transcripts produced by Pol V and chromatin remodeling factors (Zhu et al., 2013). Likewise, the interaction between IDN2 and the RPA complex spurred us to test whether IDN2 may cooperate with diRNA, paired with Pol V-dependent long noncoding RNAs, to facilitate the recruitment of RPA to DSB sites. Therefore, we examined foci formation of RPA2B-YFP in live root tip cells in the *idn2-3* mutant upon IR treatment. RPA2B-YFP readily formed IR-induced foci that are indicative of DSB sites coated with RPA (Supplemental Figure 10A). Surprisingly, the numbers of RPA2B foci in nuclei derived from the *idn2-3* mutant plants did not decrease, but significantly increased from 2 h after IR treatment and remained high 24 h after IR treatment (Figure 4A), whereas the expression levels of RPA2B-YFP were comparable in the wild-type and mutant plants (Supplemental Figure 10B). Meanwhile, the proportion of nuclei with larger number of RPA2B foci increased in the mutant background (Figure 4B). To further explore whether IDN2 functions in DSB repair through the AGO2-diRNA pathway, we observed the dynamic change of RPA2B-YFP foci in the *ago2-1* mutant. Indeed, the *AGO2* mutation also led to overaccumulated RPA2B at DSB sites and a higher proportion of nuclei containing larger number of RPA2B-YFP foci (Figures 4C and 4D), with no effects on the expression level of RPA2B-YFP (Supplemental Figure 10C).

Depletion of IDN2 or AGO2 Leads to Mislocalization of RAD51

In yeast and humans, it has been shown that RAD51 filament formation and strand invasion in HR repair were greatly inhibited due to retained RPA (Symington, 2002; Wang and Haber, 2004). To assess whether RAD51 loading downstream of RPA dissociation was affected by IDN2 or AGO2 dysfunction, we isolated nuclei of leaf cells from the RPA2B-YFP transgenic plants in the wild-type and different mutant backgrounds and co-immunostained RPA2B-YFP and RAD51. Consistently, we found increased RPA2B-YFP foci and increased proportion of cells with larger number of RPA2B-YFP foci (Figures 5A and 5B). Strikingly, distinct RAD51 foci formation was disrupted and RAD51 staining diffused in *idn2-3* and *ago2-1*, although the numbers of RAD51 foci and the proportion of cells with certain amount of RAD51 foci remained essentially unchanged (Figures 5A and 5C). As a result of defective RAD51 loading, the percentage of colocalized RPA2B-YFP and RAD51 foci correspondingly declined in *idn2-3* and *ago2-1* compared with that in the wild-type background (Figures 5A and 5D).

DISCUSSION

We previously discovered a diRNA pathway that shares some components with the RdDM pathway and facilitates HR repair (Wei et al., 2012). In this study, we show that IDN2 and its two paralogs IDP1 and IDP2, which together form a complex and are involved in RdDM (Ausin et al., 2012; Xie et al., 2012; Zhang et al., 2012), are required for HR repair (Figure 1). In addition, we found that IDN2

specifically interacts with the RPA complex (Figure 2). Although we expected that IDN2 may facilitate the recruitment of DNA repair factors, such as RPA and RAD51, like recruiting chromatin-remodeling factors in RdDM, IDN2 depletion did not cause reduced RPA and RAD51 foci formation, but led to RPA accumulation (Figure 4), aberrant formation of RAD51 foci, and decreased colocalization of RPA and RAD51 (Figure 5). This is reminiscent of the effect caused by either the knockdown of RNF4, a SUMO-targeted ubiquitin E3 ligase (Galanty et al., 2012), or the depletion of BRG1, the ATPase subunit of the SWI/SNF chromatin-remodeling complex (Qi et al., 2015), in human cells. Both also gave rise to increased RPA retention and defective RAD51 loading. RNF4 promotes RPA dissociation via regulating its turnover (Galanty et al., 2012), whereas BRG1 facilitates RPA displacement through interaction with RAD52, a key mediator involved in RPA replacement by RAD51 (Qi et al., 2015). Due to differences in the nature of IDN2, RNF4, and BRG1, it is unlikely that IDN2 mediates efficient RPA clearance and RAD51 filament assembly via the same mechanism employed by RNF4 or BRG1. Because IDN2 physically binds the RPA complex, we speculate that IDN2 binding may induce conformational change of RPA, thus reducing the ssDNA binding affinity of RPA and facilitating its dissociation from ssDNA tails. However, in light of the role of chromatin remodeling in HR (Lans et al., 2012), we could not rule out the possibility that IDN2 promotes RPA dissociation through its interacting partner, the SWI3B chromatin remodeler (Zhu et al., 2013).

IDN2 was first identified as a component in the RdDM pathway from forward genetic screens (Ausin et al., 2009; Zheng et al., 2010; Schalk et al., 2016). In the RdDM pathway, AGO4 binds siRNAs and is recruited to target loci through base pairing between the siRNAs and nascent scaffold transcripts that are generated by Pol V (Wierzbicki et al., 2008). IDN2 contains an XS domain and binds dsRNAs in vitro (Ausin et al., 2009; Zhang et al., 2012). It has been hypothesized that IDN2 binds dsRNAs formed by siRNAs pairing with their target RNAs and stabilizes the base-pairing interaction, facilitating further recruitment of downstream factors to RdDM targets (Ausin et al., 2009; Zheng et al., 2010). Supporting this hypothesis, RNA immunoprecipitation experiments indicated that IDN2 binds Pol V transcripts and that this binding requires AGO4 (Bohmdorfer et al., 2014). In this study, diRNAs were required to assist IDN2 in RPA dissociation, as AGO2 dysfunction causes the same effects as IDN2 mutation (Figures 4C and 4D) and the RNA binding activity of IDN2 may contribute to its role in DSB repair (Figures 1A, 1D, and 1E). Moreover, we have previously shown that Pol V is required for DSB repair (Wei et al., 2012). We thus hypothesize that IDN2 is guided to DSB sites by recognizing diRNAs that base pair with Pol V transcripts produced from sequences near DSB sites.

Thus, we propose a model for the role of IDN2 in diRNA-mediated HR repair (Figure 6). In our model, AGO2/diRNA complexes are recruited to DSBs through base pairing with nascent transcripts, providing dsRNA structures for IDN2 binding. IDN2 complexes interact with RPA complexes and facilitate their dissociation from DSB ends, thereby promoting the formation of RAD51 filaments that mediate HR repair. We anticipate that future studies will add to our results and continue to elucidate the biochemical mechanisms underlying IDN2-mediated RPA displacement.

METHODS

Plant Materials and Growth Conditions

All *Arabidopsis thaliana* lines used in this study are in the Columbia (Col-0) background. The DGU.US-1 line and the 2×35S:I-SceI-8 line have been previously described (Orel et al., 2003; Mannuss et al., 2010) and were provided by Holger Puchta. The *idn2-1* mutant was described previously (Ausin et al., 2009) and was obtained from Steve Jacobsen. The *idn2-3*, *idp1-1*, and *idp2-1* mutants have been described (Zhang et al., 2012) and were provided by Xinjian He. The *rpa2a-1* mutant (Xia et al., 2006) was provided by Zhizhong Gong, and *rpa1c-1*, *rpa1e-1*, *rpa2b-1*, and *rpa3a-1* were ordered from the ABRC. The transgenic plant *ProRPA2B:RPA2B-YFP-HA* was generated using the floral dip method (Clough and Bent, 1998) mediated by *Agrobacterium tumefaciens* strain GV3101. Positive transformants were identified through selection for hygromycin resistance and verified by immunoblot. All plants were grown on Murashige and Skoog plates or in soil under a 16-h-light/8-h-dark regime at 22°C/18°C, respectively.

Plasmid Construction

cDNA fragments of MRE11, RAD50, RPA1A, RPA1B, RPA1C, RPA1D, RPA1E, RPA2A, RPA2B, RPA3A, RPA3B, RAD51, and IDN2 were amplified by RT-PCR and cloned into pCambia1300-35S-N1-YFPN and pCambia1300-35S-N1-YFPC to generate constructs for the BiFC assays. To construct vectors for protoplast transformation, the coding sequences of RPA1C, RPA1E, RPA2A, RPA2B, RPA3A, RPA3B, and IDN2 were then subcloned into pCambia1300-35S-N1-YFP (Fang and Spector, 2007) and modified pCambia2300 vectors containing the 3×FLAG or 3×HA coding sequence. To express recombinant proteins, the coding sequences of IDN2 and RPA2B were amplified and inserted between the *Eco*RI and *Sal*I restriction sites in pET28a (Novagen) and pGEX-6P-1 vector, resulting in pET28a-IDN2 and pGEX-6P-1-RPA2B, respectively. A 3-kb DNA fragment containing the putative RPA2B promoter and its full-length genomic sequence was amplified and ligated into the *Kpn*I/*Bam*HI sites of a modified pCambia1301 vector containing a YFP-HA coding sequence, creating ProRPA2B:RPA2B-YFP-HA. Primers used for construction of the vectors are listed in Supplemental Table 1.

DSB Repair Reporter Assay

The DSB repair reporter assay was performed essentially as previously described (Wei et al., 2012). Briefly, the DGU.US reporter (R) line and the DSB-triggering (T) line (Orel et al., 2003; Mannuss et al., 2010) were introduced into various Arabidopsis mutant backgrounds. The progenies of RxT crossed plants were then used for GUS staining or PCR detection of the repaired *GUS* gene. For GUS staining, seedlings were infiltrated with 50 mM sodium phosphate (pH 7.0), 10 mM EDTA, and 0.5 mg/mL X-gluc (Apollo Scientific), followed by incubation at 37°C in the dark overnight. Plantlets were then cleared in ethanol, and the blue sectors in each plantlet were counted under a stereomicroscope (Nikon) and representative pictures were taken.

Small RNA Gel Blot

Total RNA was isolated from 13-d-old seedlings using the RNAiso plus kit (Takara). Small RNAs were enriched, separated on 15% denaturing PAGE gel, and transferred to a membrane. To detect small RNAs generated from the DSB region, a 444-bp PCR fragment was amplified from the DGU.US construct, randomly labeled with [α-^{32}P]dCTP, and used as probe. miR173 were probed with [γ-^{32}P]ATP-labeled DNA oligonucleotides and used as loading controls. The sequences of the primers and probes can be found in Supplemental Table 1.

Small RNA Deep Sequencing and Bioinformatic Analysis

Small RNA cloning, sequencing, and bioinformatic analysis were performed essentially as described (Wei et al., 2012). Briefly, small RNAs were separated on 15% denaturing PAGE gel, purified, and used for generating libraries for Illumina sequencing. After the removal of adaptor sequences, sequencing reads were mapped to the DGU.US sequence and perfectly matched reads were counted.

Agroinfiltration and BiFC Assay

Agroinfiltration and BiFC experiments were conducted as described (Fang and Spector, 2007) except that *Nicotiana benthamiana* leaves were used for transient expression. Briefly, agrobacteria transformed with paired YFPN and YFPC constructs were coinfiltrated into *N. benthamiana* leaves. After 48 h, infiltrated leaves were collected for fluorescence microscopy.

Protoplast Transformation

Arabidopsis protoplast isolation and PEG-mediated transformation were performed as described (Yoo et al., 2007). Briefly, protoplasts were isolated from Arabidopsis leaves and incubated with plasmids in PEG/Ca solution (40% PEG4000 [Fluka], 100 mM $CaCl_2$, and 0.2 M mannitol) for 20 min. After being washed three times with W5 solution (154 mM NaCl, 125 mM $CaCl_2$, 5 mM KCl, 5 mM glucose, and 2 mM MES, pH 5.6), the transformed protoplasts were cultured for 16 h under dim light and then harvested for protein extraction.

GST Pull-Down Assay

GST, GST-RPA2B, and His-IDN2 were expressed in *Escherichia coli* BL21 (DE3) cells and purified from the soluble fraction using glutathione agarose beads for GST and GST-RPA2B (GE Healthcare) and Ni Sepharose 6 Fast Flow for His-IDN2 (GE Healthcare). For GST pull-down experiments, 5 μg of His-IDN2 and 10 μg of GST or GST-RPA2B were incubated with 20 μL of glutathione agarose beads in binding buffer (25 mM Tris-HCl, pH 7.5, 100 mM NaCl, and 1 mM DTT) at 4°C for 2 h. The beads were washed five times using washing buffer (25 mM Tris-HCl, pH 7.5, 100 mM NaCl, 1 mM DTT, and 0.1% Triton X-100) before the protein complexes were eluted for immunoblot analysis.

Immunoprecipitation

Protoplasts or seedlings ground in liquid nitrogen were homogenized with lysis buffer (50 mM Tris-HCl, pH 7.6, 150 mM NaCl, 4 mM $MgCl_2$, 0.1% Nonidet P-40, 0.5 mM DTT, and 1 mM PMSF). After centrifugation at 12,000 rpm, the supernatant was incubated at 4°C with either GFP binding protein-conjugated beads or anti-FLAG M2 magnetic beads (Sigma-Aldrich; M8823) for 2 h. The beads were washed five times. The bound protein complexes were then eluted and subject to immunoblot analysis.

Protein Gel Blot

Total extracts or immunoprecipitates were separated using SDS-PAGE gels, transferred to PVDF membranes, and detected using antibodies against GFP (Roche; 11814460001), tubulin (Sigma-Aldrich; T5168), FLAG (Sigma-Aldrich; F1804), HA (Roche; 11666606001), GST (CWBIO; CW0291A), His (Origene; TA150088), or IDN2 (a homemade rabbit polyclonal antibody raised against the synthetic peptide N-CLLDQWEKAKRKRGMA-C).

Phylogenetic Tree Analyses

Alignment of protein sequences was performed with ClustalX (gap open penalty: 10; gap extension penalty: 0.1; protein weight matrix: BLOSUM) before MEGA (Molecular Evolutionary Genetics Analysis, version 6.0) (Tamura et al., 2013) was used for phylogenetic analysis. Evolutionary relationships were deduced using the maximum likelihood method (Saitou, 1988) with bootstrap values (10,000 replicates). Evolutionary distances were computed with the Jones-Taylor-Thornton model with default values (rate among sites: uniform rates; gap/missing data treatment: complete deletion; ML heuristic method: NNI) (Jones et al., 1992).

Immunofluorescence Staining

A transgenic line expressing RPA2B-YFP was crossed with *idn2-3* or *ago2-1* mutants. γ-Irradiation of progenies homozygous for RPA2B-YFP and *idn2-3* or *ago2-1* was performed with a Cs-137 source at an absorbed dose of 100 Gy (0.7532 ± 0.003 Gy/min). Leaf nuclei were prepared as described (Onodera et al., 2005) and co-immunostained with antibodies against RAD51 and GFP as previously described (Friesner et al., 2005; Amiard et al., 2010). Briefly, the leaf nuclei were fixed in 4% paraformaldehyde for 20 min and then incubated overnight at 4°C with primary antibodies, rabbit anti-RAD51, and mouse anti-GFP antibodies. Afterward, the nuclei preparations were incubated with Alexa 594-labeled anti-rabbit or Alexa 488-labeled anti-mouse secondary antibodies for 2 h at 37°C. DNA was counterstained using 1 μg/mL 4′,6-diamidino-2-phenylindole (DAPI) in mounting medium.

Fluorescence Microscopy

Images of the nuclei of agroinfiltrated *N. benthamiana* cells were obtained with an Axio Imager Z2 upright microscope equipped with a CCD camera (AxioCam MRm) and filters for YFP (exciter, 500/20 nm; emitter, 535/30 nm; for DAPI, exciter, 360/40 nm; emitter, 450/60 nm). To visualize RPA2B-YFP, the primary roots of RPA2B-YFP transgenic plants at the indicated time points after γ-irradiation were excised and transferred to slides. The slides were mounted in Vectashield mounting medium (Vector Laboratories) and used for confocal imaging with a Zeiss LSM 5 Pascal inverted confocal microscope (filter: exciter, 488/512 nm; emitter, 520/50 nm). The co-immunostained nuclei were visualized with a Nikon Eclipse E800i epifluorescence microscope equipped with a Photometrics Coolsnap HQ2 Mono digital camera. Images were achieved using SoftWorx software and pseudocolored and merged in Adobe Photoshop 7.

Accession Numbers

Sequence data from this study can be found in the Arabidopsis Genome Initiative database under the following accession numbers: *IDN2* (AT3G48670), *IDP1* (AT1G15910), *IDP2* (AT4G00380), *MRE11* (AT5G54260), *RAD50* (AT2G31970), *RAD51* (AT5G20850), *RPA1A* (AT2G06510), *RPA1B* (AT5G08020), *RPA1C* (AT5G45400), *RPA1D* (AT5G61000), *RPA1E* (AT4G19130), *RPA2A* (AT2G24490), *RPA2B* (AT3G02920), *RPA3A* (AT3G52630), and *RPA3B* (AT4G18590). Small RNA deep sequencing data sets generated in this study have been deposited in the National Center for Biotechnology Information Gene Expression Omnibus (http://www.ncbi.nlm.nih.gov/geo/) under accession number GSE94305. Germplasm used is as follows: *idn2-3* (SALK_152144), *idp1-1* (SALK_075378), *idp2-1* (SALK_066712), *rpa2a-1* (SALK_129173), *rpa1c-1* (SALK_085556), *rpa1e-1* (SALK_120368), *rpa2b-1* (CS851810), and *rpa3a-1* (SALK_024007).

Supplemental Data

Supplemental Figure 1. Histochemical GUS Staining Images of the T, R, and RxT Plants.

Supplemental Figure 2. Histochemical GUS Staining Images of RxT Plants in the *idn2-3* Mutant (−/−) Background or in the Corresponding Wild-Type (+/+) Background.

Supplemental Figure 3. Histochemical GUS Staining Images of RxT Plants in the *idp1-1* Mutant (−/−) Background or in the Corresponding Wild-Type (+/+) Background.

Supplemental Figure 4. Histochemical GUS Staining Images of RxT Plants in the *idp2-1* Mutant (−/−) Background or in the Corresponding Wild-Type (+/+) Background.

Supplemental Figure 5. Histochemical GUS Staining Images of RxT Plants in the *idn2-1* Mutant (−/−) Background or in the Corresponding Wild-type (+/+) Background.

Supplemental Figure 6. IDN2 Is Not Required for diRNA Production.

Supplemental Figure 7. A Screen for Interactions between IDN2 and Components of the HR Repair Pathway by BiFC.

Supplemental Figure 8. Maximum Likelihood Phylogenetic Trees Showing the Relationships among RPA Proteins.

Supplemental Figure 9. Detection of Interaction between RPA2B and Other RPA Subunits by BiFC.

Supplemental Figure 10. RPA2B-YFP Form Foci in Plant Root Cells Treated with γ-Irradiation.

Supplemental Table 1. Oligonucleotides Used in This Study

Supplemental File 1. Text File of the Sequences and Alignments Used for the Phylogenetic Analyses Shown in Supplemental Figure 8.

ACKNOWLEDGMENTS

We thank L. Du and J. Su for assistance with γ-irradiation treatments and to Q. Feng for advice on confocal microscopy. This work was supported by grants from National Key Research and Development Program of China (Grant 2016YFA0500800) and the National Science Foundation of China (Grants 31421001 and 31330042) to Y.Q.

AUTHOR CONTRIBUTIONS

M.L., Z.B., and Y.Q. conceived and designed the experiments. M.L., Z.B., P.C.-N., W.W., O.P., F.K., and L.L. performed the experiments. M.L., O.P., Y.L., J.C., and Y.Q. analyzed the data. M.L., Y.L., and Y.Q. wrote the article.

Received October 5, 2016; revised January 17, 2017; accepted February 17, 2017; published February 21, 2017.

REFERENCES

Aklilu, B.B., Soderquist, R.S., and Culligan, K.M. (2014). Genetic analysis of the Replication Protein A large subunit family in Arabidopsis reveals unique and overlapping roles in DNA repair, meiosis and DNA replication. Nucleic Acids Res. **42:** 3104–3118.

Amiard, S., Charbonnel, C., Allain, E., Depeiges, A., White, C.I., and Gallego, M.E. (2010). Distinct roles of the ATR kinase and the Mre11-Rad50-Nbs1 complex in the maintenance of chromosomal stability in Arabidopsis. Plant Cell **22:** 3020–3033.

Ausin, I., Mockler, T.C., Chory, J., and Jacobsen, S.E. (2009). IDN1 and IDN2 are required for de novo DNA methylation in *Arabidopsis thaliana*. Nat. Struct. Mol. Biol. **16:** 1325–1327.

Ausin, I., et al. (2012). INVOLVED IN DE NOVO 2-containing complex involved in RNA-directed DNA methylation in Arabidopsis. Proc. Natl. Acad. Sci. USA **109:** 8374–8381.

Bohmdorfer, G., Rowley, M.J., Kucinski, J., Zhu, Y., Amies, I., and Wierzbicki, A.T. (2014). RNA-directed DNA methylation requires stepwise binding of silencing factors to long non-coding RNA. Plant J. **79:** 181–191.

Chen, R., and Wold, M.S. (2014). Replication protein A: single-stranded DNA's first responder: dynamic DNA-interactions allow replication protein A to direct single-strand DNA intermediates into different pathways for synthesis or repair. BioEssays **36:** 1156–1161.

Ciccia, A., and Elledge, S.J. (2010). The DNA damage response: making it safe to play with knives. Mol. Cell **40:** 179–204.

Clough, S.J., and Bent, A.F. (1998). Floral dip: a simplified method for Agrobacterium-mediated transformation of *Arabidopsis thaliana*. Plant J. **16:** 735–743.

Culligan, K.M., Robertson, C.E., Foreman, J., Doerner, P., and Britt, A.B. (2006). ATR and ATM play both distinct and additive roles in response to ionizing radiation. Plant J. **48:** 947–961.

Eschbach, V., and Kobbe, D. (2014). Different replication protein A complexes of *Arabidopsis thaliana* have different DNA-binding properties as a function of heterotrimer composition. Plant Cell Physiol. **55:** 1460–1472.

Fang, X., and Qi, Y. (2016). RNAi in plants: An Argonaute-centered view. Plant Cell **28:** 272–285.

Fang, Y., and Spector, D.L. (2007). Identification of nuclear dicing bodies containing proteins for microRNA biogenesis in living Arabidopsis plants. Curr. Biol. **17:** 818–823.

Francia, S., Michelini, F., Saxena, A., Tang, D., de Hoon, M., Anelli, V., Mione, M., Carninci, P., and d'Adda di Fagagna, F. (2012). Site-specific DICER and DROSHA RNA products control the DNA-damage response. Nature **488:** 231–235.

Friesner, J.D., Liu, B., Culligan, K., and Britt, A.B. (2005). Ionizing radiation-dependent gamma-H2AX focus formation requires ataxia telangiectasia mutated and ataxia telangiectasia mutated and Rad3-related. Mol. Biol. Cell **16:** 2566–2576.

Fukunaga, R., and Doudna, J.A. (2009). dsRNA with 5′ overhangs contributes to endogenous and antiviral RNA silencing pathways in plants. EMBO J. **28:** 545–555.

Galanty, Y., Belotserkovskaya, R., Coates, J., and Jackson, S.P. (2012). RNF4, a SUMO-targeted ubiquitin E3 ligase, promotes DNA double-strand break repair. Genes Dev. **26:** 1179–1195.

Gao, M., et al. (2014). Ago2 facilitates Rad51 recruitment and DNA double-strand break repair by homologous recombination. Cell Res. **24:** 532–541.

Jones, D.T., Taylor, W.R., and Thornton, J.M. (1992). The rapid generation of mutation data matrices from protein sequences. Comput. Appl. Biosci. **8:** 275–282.

Krejci, L., Altmannova, V., Spirek, M., and Zhao, X. (2012). Homologous recombination and its regulation. Nucleic Acids Res. **40:** 5795–5818.

Lans, H., Marteijn, J.A., and Vermeulen, W. (2012). ATP-dependent chromatin remodeling in the DNA-damage response. Epigenetics Chromatin **5:** 4.

Law, J.A., and Jacobsen, S.E. (2010). Establishing, maintaining and modifying DNA methylation patterns in plants and animals. Nat. Rev. Genet. **11:** 204–220.

Lieber, M.R. (2010). The mechanism of double-strand DNA break repair by the nonhomologous DNA end-joining pathway. Annu. Rev. Biochem. **79:** 181–211.

Mannuss, A., Dukowic-Schulze, S., Suer, S., Hartung, F., Pacher, M., and Puchta, H. (2010). RAD5A, RECQ4A, and MUS81 have specific functions in homologous recombination and define different pathways of DNA repair in *Arabidopsis thaliana*. Plant Cell **22:** 3318–3330.

Matzke, M.A., and Mosher, R.A. (2014). RNA-directed DNA methylation: an epigenetic pathway of increasing complexity. Nat. Rev. Genet. **15:** 394–408.

Mimitou, E.P., and Symington, L.S. (2008). Sae2, Exo1 and Sgs1 collaborate in DNA double-strand break processing. Nature **455:** 770–774.

Moynahan, M.E., and Jasin, M. (2010). Mitotic homologous recombination maintains genomic stability and suppresses tumorigenesis. Nat. Rev. Mol. Cell Biol. **11:** 196–207.

Onodera, Y., Haag, J.R., Ream, T., Costa Nunes, P., Pontes, O., and Pikaard, C.S. (2005). Plant nuclear RNA polymerase IV mediates siRNA and DNA methylation-dependent heterochromatin formation. Cell **120:** 613–622.

Orel, N., Kyryk, A., and Puchta, H. (2003). Different pathways of homologous recombination are used for the repair of double-strand breaks within tandemly arranged sequences in the plant genome. Plant J. **35:** 604–612.

Puchta, H. (2005). The repair of double-strand breaks in plants: mechanisms and consequences for genome evolution. J. Exp. Bot. **56:** 1–14.

Qi, W., Wang, R., Chen, H., Wang, X., Xiao, T., Boldogh, I., Ba, X., Han, L., and Zeng, X. (2015). BRG1 promotes the repair of DNA double-strand breaks by facilitating the replacement of RPA with RAD51. J. Cell Sci. **128:** 317–330.

Qi, Y., He, X., Wang, X.J., Kohany, O., Jurka, J., and Hannon, G.J. (2006). Distinct catalytic and non-catalytic roles of ARGONAUTE4 in RNA-directed DNA methylation. Nature **443:** 1008–1012.

Saitou, N. (1988). Property and efficiency of the maximum likelihood method for molecular phylogeny. J. Mol. Evol. **27:** 261–273.

San Filippo, J., Sung, P., and Klein, H. (2008). Mechanism of eukaryotic homologous recombination. Annu. Rev. Biochem. **77:** 229–257.

Sartori, A.A., Lukas, C., Coates, J., Mistrik, M., Fu, S., Bartek, J., Baer, R., Lukas, J., and Jackson, S.P. (2007). Human CtIP promotes DNA end resection. Nature **450:** 509–514.

Schalk, C., et al. (2016). DNA DAMAGE BINDING PROTEIN2 (DDB2) shapes the DNA methylation landscape. Plant Cell **28:** 2043–2059.

Symington, L.S. (2002). Role of RAD52 epistasis group genes in homologous recombination and double-strand break repair. Microbiol. Mol. Biol. Rev. **66:** 630–670.

Tamura, K., Stecher, G., Peterson, D., Filipski, A., and Kumar, S. (2013). MEGA6: Molecular Evolutionary Genetics Analysis version 6.0. Mol. Biol. Evol. **30:** 2725–2729.

van den Bosch, M., Bree, R.T., and Lowndes, N.F. (2003). The MRN complex: coordinating and mediating the response to broken chromosomes. EMBO Rep. **4:** 844–849.

Wang, X., and Haber, J.E. (2004). Role of Saccharomyces single-stranded DNA-binding protein RPA in the strand invasion step of double-strand break repair. PLoS Biol. **2:** E21.

Wei, W., Ba, Z., Gao, M., Wu, Y., Ma, Y., Amiard, S., White, C.I., Rendtlew Danielsen, J.M., Yang, Y.G., and Qi, Y. (2012). A role for small RNAs in DNA double-strand break repair. Cell **149:** 101–112.

Wendte, J.M., and Pikaard, C.S. (2017). The RNAs of RNA-directed DNA methylation. Biochim. Biophys. Acta **1860:** 140–148.

Wierzbicki, A.T., Haag, J.R., and Pikaard, C.S. (2008). Noncoding transcription by RNA polymerase Pol IVb/Pol V mediates transcriptional silencing of overlapping and adjacent genes. Cell **135:** 635–648.

Xia, R., Wang, J., Liu, C., Wang, Y., Wang, Y., Zhai, J., Liu, J., Hong, X., Cao, X., Zhu, J.K., and Gong, Z. (2006). ROR1/RPA2A, a putative replication protein A2, functions in epigenetic gene silencing and in regulation of meristem development in Arabidopsis. Plant Cell **18:** 85–103.

Xie, M., Ren, G., Costa-Nunes, P., Pontes, O., and Yu, B. (2012). A subgroup of SGS3-like proteins act redundantly in RNA-directed DNA methylation. Nucleic Acids Res. **40:** 4422–4431.

Yoo, S.D., Cho, Y.H., and Sheen, J. (2007). Arabidopsis mesophyll protoplasts: a versatile cell system for transient gene expression analysis. Nat. Protoc. **2:** 1565–1572.

Zhang, C.J., Ning, Y.Q., Zhang, S.W., Chen, Q., Shao, C.R., Guo, Y.W., Zhou, J.X., Li, L., Chen, S., and He, X.J. (2012). IDN2 and its paralogs form a complex required for RNA-directed DNA methylation. PLoS Genet. **8:** e1002693.

Zhang, H., and Zhu, J.K. (2011). RNA-directed DNA methylation. Curr. Opin. Plant Biol. **14:** 142–147.

Zheng, Z., Xing, Y., He, X.J., Li, W., Hu, Y., Yadav, S.K., Oh, J., and Zhu, J.K. (2010). An SGS3-like protein functions in RNA-directed DNA methylation and transcriptional gene silencing in Arabidopsis. Plant J. **62:** 92–99.

Zhu, Y., Rowley, M.J., Böhmdorfer, G., and Wierzbicki, A.T. (2013). A SWI/SNF chromatin-remodeling complex acts in noncoding RNA-mediated transcriptional silencing. Mol. Cell **49:** 298–309.

Zilberman, D., Cao, X., and Jacobsen, S.E. (2003). ARGONAUTE4 control of locus-specific siRNA accumulation and DNA and histone methylation. Science **299:** 716–719.